

Matthew D. Parker*

Colorado State University, Fort Collins, Colorado

1. INTRODUCTION AND BACKGROUND

Mesoscale convective systems (MCSs) account for numerous flash floods, and the flooding that they cause is related to their organizational modes and speeds. Recent work by Parker and Johnson (2000, hereafter PJ00) identified three linear MCS modes in the central U.S.: those with convective lines and either trailing, leading, or parallel precipitation, the latter two of which have received comparatively little study. This article describes idealized numerical simulations of convective lines with leading precipitation; PJ00 called these “LS” (leading stratiform) systems.

PJ00 found that, on average, LS MCSs had mean lower tropospheric inflow that passed through their pre-line precipitation. The present work focuses on these “front-fed” LS (FFLS) systems, whose survival is somewhat mysterious given the water loading and evaporative chilling of their inflow. The dynamics of FFLS systems are also interesting because, although PJ00 found environmental rear-to-front storm-relative flow in the middle and upper troposphere for FFLS MCSs, the importance of the vertical wind shear remained unclear. This article emphasizes the importance of an FFLS system’s overturning updraft, which comprises moist lower and middle tropospheric air and feeds the leading precipitation region; describing the dynamics of this overturning updraft is tantamount to describing why FFLS systems develop.

This study incorporated the Advanced Regional Prediction System (ARPS), version 4.5.2, configured in an idealized manner, with a mean midlatitude MCS temperature sounding and a mean wind profile for four archetypal FFLS systems from the PJ00 MCS population. The basic model configuration was summarized by Parker and Johnson (2001, hereafter PJ01); please contact the author for more detail. Although this study included both 2D and 3D simulations, for the sake of brevity the results described in this article are solely from the 2D simulations.

*Corresponding author address: Matthew D. Parker, Department of Geosciences, University of Nebraska–Lincoln, 214 Bessey Hall, Lincoln, NE 68588–0340. E-mail: mparker@papagayo.unl.edu
 Current affiliation: Department of Geosciences, University of Nebraska–Lincoln, Lincoln, Nebraska.

2. THEORY AND DEFINITIONS

The pressure perturbation can be decomposed as:

$$p' = p'_B + p'_{DL} + p'_{DNL}, \quad (1)$$

wherein p'_B is the component due to buoyancy, p'_{DL} is the linear part of the component due to dynamic effects, and p'_{DNL} is the nonlinear part of the component due to dynamic effects. For the anelastic set (also neglecting Coriolis and frictional accelerations), the diagnostic equations for these pressure components in 2D are:

$$\nabla^2 p'_B = \frac{\partial}{\partial z} (\rho_o B); \quad (2)$$

$$\nabla^2 p'_{DL} = -2\rho_o \frac{du_o}{dz} \frac{\partial w}{\partial x}. \quad (3)$$

$$\begin{aligned} \nabla^2 p'_{DNL} = & -\rho_o \left[\left(\frac{\partial u'}{\partial x} \right)^2 + \left(\frac{\partial w}{\partial z} \right)^2 \right. \\ & \left. - w^2 \frac{\partial^2}{\partial z^2} (\ln \rho_o) \right] - 2\rho_o \frac{\partial u'}{\partial z} \frac{\partial w}{\partial x}; \end{aligned} \quad (4)$$

wherein $B \equiv -g\rho'/\rho_o$ is buoyancy. Accelerations can be attributed to the horizontal and vertical gradients in p'_B , p'_{DL} , and p'_{DNL} , as well as to B . Hereafter, these components of acceleration are abbreviated as ACC_B (including both B and the gradients in p'_B), ACC_{DL} , and ACC_{DNL} . A brief discussion of these pressure perturbations and accelerations in a simulated FFLS system follows.

3. MEAN STATE AND TRANSIENT DYNAMICS

On average, during the mature phase of the simulated FFLS system, air below ≈ 6 km AGL flows westward and passes through a pre-line region of cloud and precipitation on its way to the convective region (Fig. 1). As shown by PJ01, some of this inflowing air ascends and feeds deep convective updrafts while the remainder passes through the line’s mean position and contributes to the surface cold pool. Although it isn’t clear from Fig. 1, trajectories confirm that lower tropospheric air does participate in the deep convective updrafts (Fig. 2; also see PJ01).

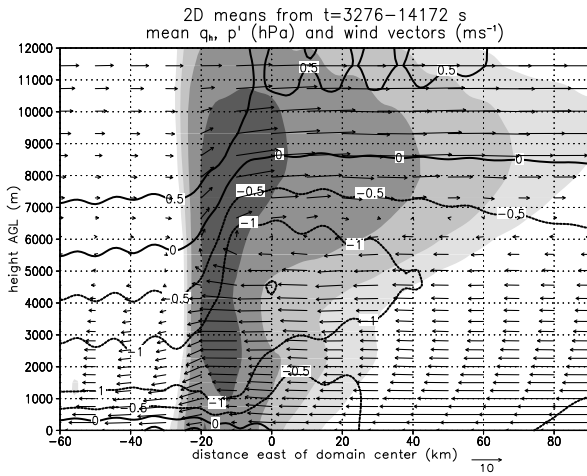


Figure 1: Mean total hydrometeor mixing ratio (levels of shading are 0.02, 0.08, 0.32, 1.28, and 5.12 g kg^{-1}), pressure perturbation (contours, hPa), and wind vectors (m s^{-1} , scaled as shown) for control simulation.

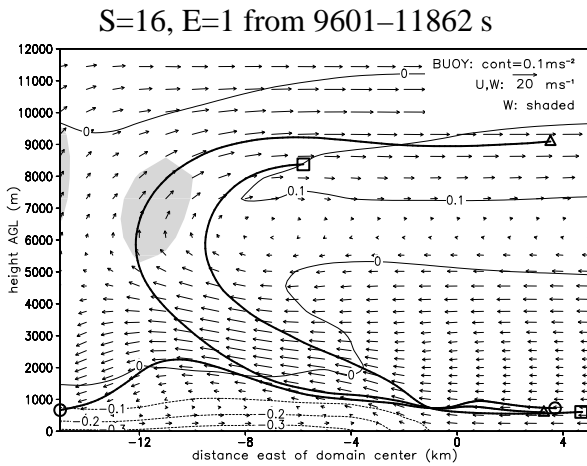


Figure 2: Segments of the three representative air parcel trajectories, plotted as bold curves for control ($S=16, E=1$) simulation from 9601–11862 s. Parcels' symbols (Δ , \circ , and \square) indicate their positions at starting and ending times of the figure. Also plotted: mean B (contours), u and w (vectors), with w shaded at 5 m s^{-1} .

As shown in Fig. 2, three air parcels (Δ , \circ , and \square) that approach the convective region with very similar trajectories and pass through the exact same point ($x = -1 \text{ km}, z = 730 \text{ m AGL}$) at different times (Δ at $t = 10196 \text{ s}$, \circ at $t = 10315 \text{ s}$, and \square at 11148 s) follow markedly different trajectories through and away from the convective region. By inspecting the temporally averaged fields in Fig. 2, it is impossible to determine why some air parcels ascend in the deep updrafts (i.e. Δ and \square) while others do not (i.e. \circ).

Updrafts in the FFLS simulations are alternately produced and suppressed. Although it is not feasible in this brief article to display plots of the p' and ACC compo-

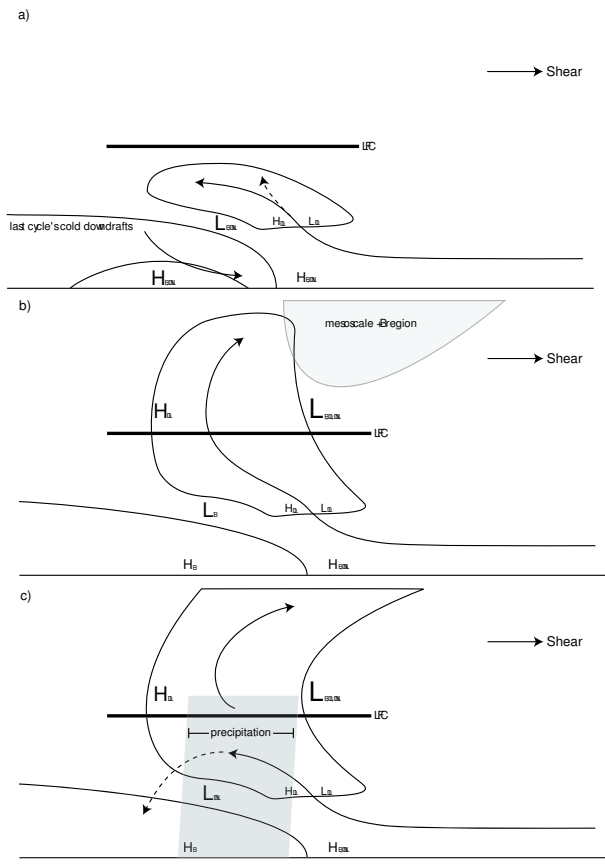


Figure 3: Schematic depiction of the FFLS multicellular cycle. a) development of a fresh updraft at the outflow boundary/gust front. b) maturation of the overturning updraft. c) the updraft is cut off from the inflow by precipitation. The cold pool and cloud outlines are shown schematically, along with typical airstreams. Pressure maxima and minima are shown with “H” and “L” characters: their sizes indicate approximate magnitudes and their subscripts indicate the pressure components to which they are attributed.

nents at numerous times, the general cycle is as follows.

1) Early in the lifetime of a new updraft, lifting at the edge of the cold pool is enhanced by ACC_B and ACC_{DNL} (Fig. 3a); this enhancement is largely due to a surge of outflow from the previous convective cycle, which strengthens the cold pool and intensifies the convergence at the gust front. Air parcels are decelerated as they approach the gust front, providing an extended period of time for the upward accelerations to impart positive w to the inflowing air parcels. Once air parcels have ascended over the outflow boundary, they are accelerated strongly rearward owing to the horizontal gradients in p'_{DNL} and p'_B . Often, the horizontal ACC_B is attributable to a p'_B minimum below a developing cloud.

2) As the updraft continues to develop at low levels, a downshear-directed ACC_{DL} helps to provide more erect trajectories (the dashed arrow in Fig. 3a). The more erect updraft allows air to spend more time in the

zone of upward acceleration, and decreases the magnitude of the minimum in p'_{DNL} over the cold pool head (the weakening of the old downdrafts also is relevant to this decrease). During the active phase of the multicell, many air parcels are lifted to their LFCs, participate in the main updraft, and are accelerated downshear by some combination of ACC_B , ACC_{DNL} , and ACC_{DL} (Fig. 3b). For example, as Δ enters the active updraft between 10672 and 10910 s of the FFLS simulation, ACC_B , ACC_{DNL} , and ACC_{DL} all are directed downshear and have similar magnitudes (Fig. 4). The downshear minima in p'_B and p'_{DNL} are partly related to the mesoscale buoyancy and wind perturbations, and hence represent a feedback whereby the FFLS structure reinforces the overturning nature of the updrafts. Hence, in a mature FFLS system, the effect of the mean vertical wind shear (i.e. ACC_{DL}) alone doesn't predominate.

3) The system deviates from the classical trailing precipitation model in that cloud and precipitation particles are carried forward from the convective updraft owing to air parcels' large net downshear accelerations. Therefore, as the convective updraft's life span progresses, some precipitation begins to fall in advance of the updraft's position. Eventually there is a point of cut-off, when inflowing air parcels experience downward accelerations owing to hydrometeor loading as they approach the updraft. As their vertical velocities decrease, they require longer and longer times to reach an LFC, and eventually move almost horizontally and accumulate downward acceleration until they descend (Fig. 3c). At this point, the multicell is suppressed, and no additional inflowing air parcels join the updraft. Meanwhile, the inflowing air parcels that have been strongly accelerated downward compose a downdraft and surge of outflow that strengthens the cold pool. Once the newly cut-off updraft has decayed and the precipitation curtain has dissipated sufficiently, the stage is once again set for phase 1 (i.e. for panel a of Fig. 3).

4. DESTABILIZATION OF INFLOW

As inflowing air passes through the pre-line precipitation, it is cooled owing to evaporation, melting, and ascent, much as PJ00 speculated. However, an important result of the present study is that this cooling occurs over a relatively deep layer and destabilizes the near-line sounding (Fig. 5), rendering diminished CIN and increased CAPE.

Leading precipitation provides two beneficial effects, both of which tend to destabilize the near-line sounding. 1) The leading precipitation melts and evaporates as it falls into the inflow, rendering cooling that increases with height over the lowest 2-2.5 km AGL (Fig. 6 a,b). Notably, Fig. 6b implies that the lowest 1 km of the in-

S=16, E=1 from 10672–10910 s

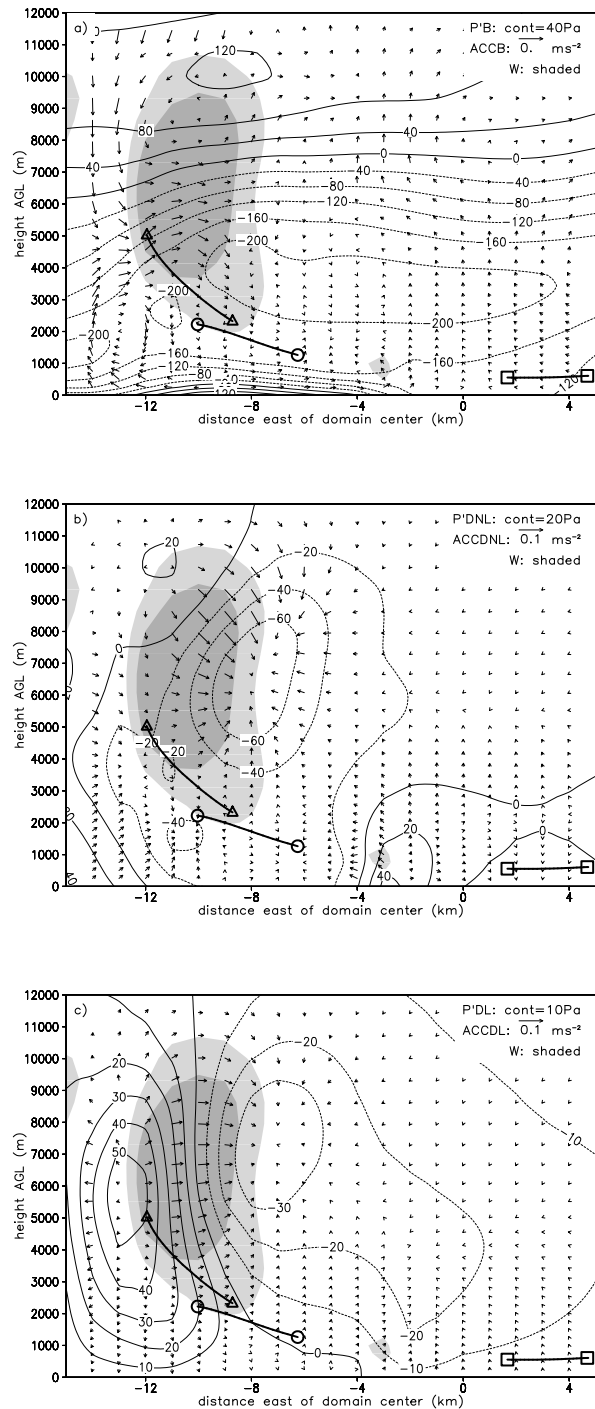


Figure 4: Subset of trajectories in Fig. 2 for control (S=16, E=1) simulation from 10672–10910 s: a) p'_B contoured, ACC_B vectors. b) p'_{DNL} contoured, ACC_{DNL} vectors. c) p'_{DL} contoured, ACC_{DL} vectors. w is shaded in all panels at 5 and 10 $m s^{-1}$.

flow layer ought to be stabilized near the convective line by decreasing evaporation with height. However, the

detriment of this process is minimal because inflow in the lowest 1 km AGL is moving westward rapidly, and therefore doesn't spend much time in the region of significant chilling. 2) As widespread evaporation and melting ensue, they lead to a p'_B field that induces upward accelerations on inflowing air parcels in and ahead of the leading precipitation region, which also destabilizes the inflowing layer (Fig. 6c). Notably, the very near-line environment is characterized by subsident warming that increases with height (Fig. 6c), such that the evaporation and melting terms must compensate for it if the inflowing air is to remain or become increasingly destabilized; the melting contribution proves quite helpful in this regard (Fig. 6b).

5. SUMMARY

This article summarizes idealized numerical simulations of convective lines with leading precipitation, and discusses their dynamics. Although relatively strong wind shear in the middle and upper troposphere accounts for a component of the downshear accelerations of air parcels in the simulated updrafts (ACC_{DL}), a mature system with leading precipitation also renders both persistent and periodic pressure anomalies that contribute just as much to the downshear accelerations (via ACC_B and ACC_{DNL}). Many of these accelerations, which govern the overall system structure, are transient and are lost when averaged over multiple convective cycles. An important finding is that, contrary to expectations, inflowing air is actually destabilized as it passes through the pre-line precipitation. As a result, systems with inflow passing through their line-leading precipitation can be stable and long-lived.

REFERENCES

Parker, M.D., and R.H. Johnson, 2000: Organizational modes of mid-latitude mesoscale convective systems. *Mon. Wea. Rev.*, **128**, 3413–3436.

Parker, M.D., and R.H. Johnson, 2001: Simple numerical simulations of convective lines with leading stratiform precipitation. Preprints, *Ninth Conference on Mesoscale Processes*, Fort Lauderdale, FL, 283–287.

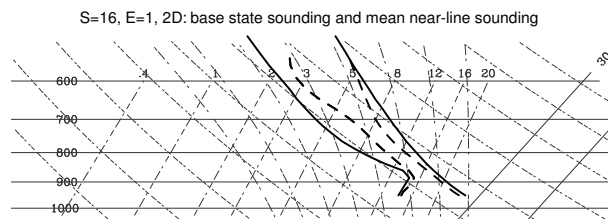


Figure 5: Skew- T ln- p diagram of the lower troposphere for base state initial condition (solid) and mean near-line sounding (dashed) for mature stage of control ($S=16$, $E=1$) simulation, averaged from 9600–14122 s.

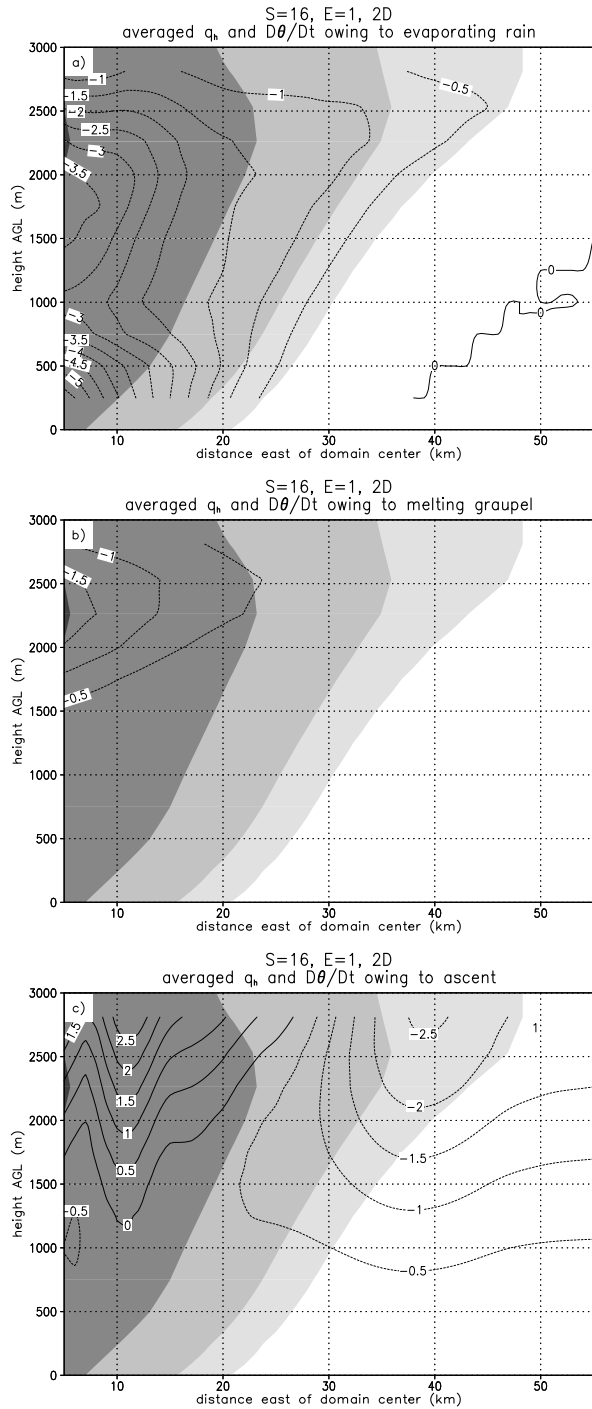


Figure 6: Mean hydrometeor mixing ratio (levels of shading are 0.005, 0.02, 0.08, and 1.28 g kg^{-1}) for control ($S=16$, $E=1$) simulation, averaged from 9600–14122 s, along with: a) heating/chilling rate owing to evaporation of falling rain (K h^{-1}), b) heating/chilling rate owing to melting of falling graupel (K h^{-1}), and c) warming/cooling rate owing to mean descent/ascent (contours, K h^{-1}).

The NSF funded this work under grant ATM-0071371. The author gratefully acknowledges the input and support of Dr. Richard Johnson.